Analysis of Film Cooling for a 3kN LOX/butane Demonstrator Engine

Z A R Ashford

Cranfield Air and Space Propulsion Institute, Cranfield University, MK43 0AL, UK

Zoe.ashford@cranfield.ac.uk

Abstract. Regenerative cooling has been the primary cooling method for every modern launch vehicle engine, except for the Viking: a film-cooled (with ablative throat) N_2O_4 / UH25 engine used on the first stage of the Ariane rockets 2-4. Despite this, film-cooling as a stand-alone cooling method has traditionally been considered insufficient for the high combustion temperatures and long burn times associated with launcher engines. This study explored the feasibility of a solely film-cooled engine at the demonstrator scale (3 kN), as a prototype for a lightweight launcher engine. A wide range of liquid oxygen (LOX)/butane engines were modelled and from this a relationship was determined to predict chamber wall temperature for a given oxidiser-to-fuel ratio (O/F), chamber pressure, and amount of film cooling. Notably, this equation was found to apply to both a 3 kN and a 30 kN engine. Numerical modelling of engine specific impulse (Isp) using this equation then found the conditions yielding optimal engine performance.

1. Introduction

Regenerative cooling has been the primary cooling method for every modern launch vehicle engine, except for the Viking: a film-cooled (with ablative throat) N_2O_4 / UH25 engine used on the first stage of the Ariane rockets 2-4. Despite this, film-cooling (as a stand-alone cooling method) has traditionally been considered insufficient for the high combustion temperatures and long burn times associated with launcher engines.

For small launch vehicles, the regenerative cooling pipework can comprise a significant proportion of the overall engine mass; by contrast, a film-cooling injection manifold is much lighter. However, film cooling has also been neglected on smaller projects. The Delft Aerospace Rocket Engineering (DARE) cryogenics project and its successor, Project Sparrow, both rely predominantly on regenerative cooling [1, 2]. For motors requiring a simpler chamber design, ablative cooling is frequently used instead [3].

Therefore, the purpose of this study was to investigate whether a 3 kN LOX/hydrocarbon engine could be cooled through film cooling alone without a significant reduction in performance, and to provide some method for determining which engine parameters would give optimal engine performance.

1.1. *Chamber conditions*

Performance losses tend to be higher in film-cooled engines than regeneratively cooled engines due to factors such as mixing losses and the loss of impulse from nonreacting fuel. From experimental data for low coolant flow rates, the reduction in I_{sp} was found to be roughly proportional to the film fraction [4].

A study of film cooling in a LOX/LH_2 engine found that the film cooling efficiency was maximised when the film consisted solely of LH_2 [5] and thus a film consisting of only fuel was chosen.

An engine operating above the propellants' critical points does not suffer losses due to heat of vaporisation: the critical pressure of n-butane is 3.8 MPa, therefore the minimum engine chamber pressure explored was 3.8 MPa. (The critical temperature of butane is 425 K, significantly lower than any likely engine operating temperature) [6, 7].

1.2. *Chamber material selection*

Preliminary studies estimated that the uncooled chamber temperature could exceed 3500 K in the engine, and it was desirable to maximise the target chamber wall temperature to minimize the film cooling required. Materials such as tungsten and several carbides have high melting points, but these were not considered to be economic and some, such as the carbides, bring manufacturing difficulties [4]. Ceramic thrust chambers have also been tested [8] but are not accessible for student-scale demonstrator engines. Copper and its alloys are frequently used due to their high thermal conductivity. However, the yield strength of copper rapidly decreases with temperature, from 5.5 MPa at 920 K (1200°F) to 4.1 MPa at 1090 K (1500°F), and this poses a significant risk for higher chamber pressures [9].

By contrast, Inconel has far superior performance: the yield strength of Inconel-625 is 380 MPa at 1030 K (1400°F), and for Inconel-718 is 758 MPa at the same temperature [10, 11]. Therefore, the use of Inconel-718 would allow a thinner chamber wall and improved high-temperature performance. To provide a reasonable safety margin, the target chamber wall temperature was then estimated as 80% of this temperature (1400°F), hence 1120 °F or 875 K.

It was assumed that a single block of graphite would be used for the nozzle and throat of the thrust chamber, as a cost-effective material to withstand the higher temperature at the throat and to ensure a seamless transition into the nozzle [4].

2. Methodology

2.1. Design Parameter Determination

Modelling was carried out in the software RPA (Rocket Propulsion Analysis) to evaluate engine performance for a range of O/F ratios and chamber pressures [12]. The results were processed using curve-fitting software CurveExpert Pro [13] to find empirical relationships for key parameters such as characteristic velocity, C*, and engine chamber temperature, T_c, as functions of the independent variables O/F ratio and chamber pressure. A full list of the equations can be found in [14]. Due to the shift in reaction regime around O/F 1.2, O/F ratios greater than and less than 1.2 had to be modelled separately as there were no equations that adequately represented the whole data set.

For C* and T_c, which were influenced significantly by both O/F and chamber pressure, rudimentary multivariable equations were developed: these returned results typically within 0.1% of random simulation data. Finally, flow compositions of both the engine core and the film were recorded in preparation for the heat transfer modelling.

2.2. Engine Design

For thrust chamber and nozzle design methods, Huzel & Huang *Modern Engineering for Design of Liquid-Propellant Rocket Engines* and Humble's *Space Propulsion, Analysis, and Design* were used [15, 16]. From these, design parameters such as characteristic length L*, contraction ratio R_c, and parabolic nozzle entry and exit angles were found. Following the creation of the design parameter relationships, an initial engine model was created to provide inputs into the HT31 program using these literature methods and constants.

2.3. Heat Transfer Modelling

Limited experimental and detailed numerical studies are available for film cooling [17] although techniques using computational fluid dynamics (CFD) are increasingly being used and validated [18, 5].

Due to the time limitations of this project, it was decided to use the Heat Transfer (HT) 31 programs developed by Professor Bob Parkinson, which were specifically designed to model film cooling in rocket engines [19]. The results from the heat transfer simulations were then analysed using AGARDograph No. 148, on which HT31 is based [20].

At this stage, the distinction was made between the overall O/F ratio of the engine, and the core O/F ratio. The addition of film cooling, which was almost entirely comprised of the fuel (butane), clearly had an impact on the overall engine O/F. However, for the HT31 program it was important to distinguish between the properties of the core flow with its core O/F, used to calculate parameters such as T_c, and the film flow, which was variable.

3. Results and Discussion

3.1. *Minimum film cooling calculation*

The film mass flow rate, $\dot{m}_{film}$, was calculated from the overall engine mass flow rate, $\dot{m}_{total}$, and used to estimate the Reynolds number at the film injection slot, Re_s, with the dynamic viscosity taken as 6 x 10^{-5} Ns/m^2. The film efficiency η was then calculated for each point along the engine. The assumption was made that the slot velocity was the same as the velocity of the fluid at the core of the engine, i.e. that $u_c/u_m = 1$ [20].

$$\eta = \frac{T_{aw} - T_c}{T_s - T_c} = \frac{Re_s}{Re_s + 0.107 f(u) Re_x^{0.8}} \qquad 1$$

$$\text{where } f(u) = 1 + 0.4 \tan^{-1}\left(\frac{u_m}{u_s} - 1\right) \text{ for } \frac{u_s}{u_m} \leq 1.0$$

Where T_c was the engine core temperature, T_{aw} the adiabatic wall temperature, and T_s the temperature of the film at the injection slot. It was assumed that the film would be injected directly from the propellant storage tank, so a temperature of 300 K was reasonable. T_{aw} was then calculated for each point along the chamber wall, defined as the region up to but not including the throat cone: in the throat cone the flow was accelerated and the equation for film efficiency in terms of Reynolds number was no longer valid. The maximum adiabatic wall temperature $T_{aw,max}$ was therefore defined as the adiabatic wall temperature immediately prior to the throat cone.

The analysis of individual HT31 outputs provided a list of $T_{aw,max}$ values for a range of core O/F ratios, chamber pressures, and film cooling amounts. Figure 1 shows the maximum adiabatic wall temperature for a range of film cooling and chamber pressures at a core O/F ratio of 2.20.

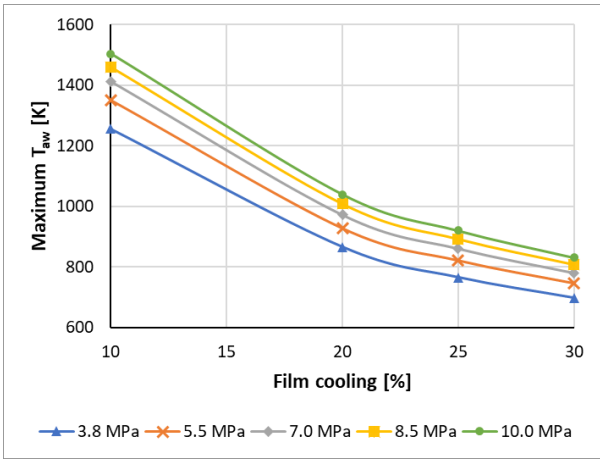

Figure 1: Maximum adiabatic wall temperature for various chamber pressures and film cooling with O/F = 2.20

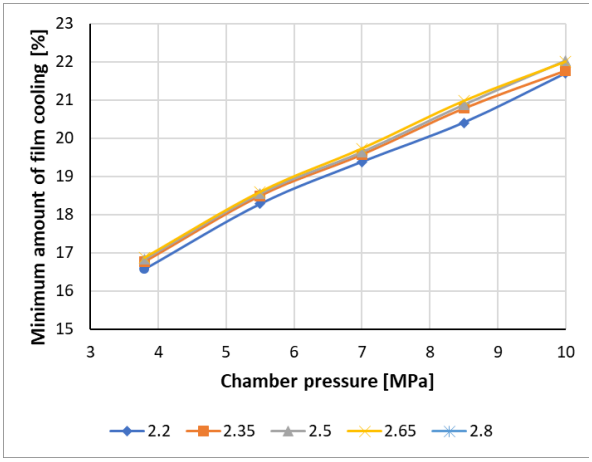

Figure 2: Minimum amount of film cooling required for a maximum adiabatic wall temperature of 1000 K

Linear interpolation was used to estimate the minimum percentage of film cooling required to achieve a specific wall temperature for each combination of pressure and core O/F ratio. Figure 2 shows the minimum amount of film cooling (%FC) needed to achieve an adiabatic wall temperature of 1000 K for a range of core O/F ratios and chamber pressures.

3.2. *Development of film cooling prediction equation*

It was found that a linear equation could be used to express the relationship between the proportion of film cooling, core O/F, chamber pressure, and target adiabatic wall temperature when the target adiabatic wall temperature was normalized by the engine core temperature – i.e T_{aw} / T_c. The relationship was then found to be:

$$\frac{T_{aw}}{T_c} = a + bR_{OF} + cP_c + d\%FC \qquad 2$$

Where R_{OF} is the O/F ratio, P_c is the chamber pressure, %FC is the percentage of film cooling with respect to the overall mass flow rate, and a, b, c, and d are coefficients. This equation could then be rearranged to give the amount of film cooling required for a given target adiabatic wall temperature:

$$\%FC = \frac{1}{d}\left(\frac{T_{aw}}{T_c} - a - bR_{OF} - cP_c\right) \qquad 3$$

While this relationship was a linear combination of parameters, it was not itself a linear function. T_c was calculated using exponential functions of both O/F and chamber pressure, and thus it was preferable to determine surface features numerically, rather than analytically.

10 of these tests met the design thrust of 3 kN, and 5 additional tests had a design thrust of 30 kN to ascertain whether the relationship was valid for a larger engine. When the 15 scenarios were modelled using the HT31 program, the calculated maximum chamber adiabatic wall temperature was typically 5-8% lower than the T_{aw} that had been used to calculate the input %FC. This indicated that the relationship was over-estimating the quantity of film cooling required.

Corrected values of the coefficients were then determined and used to predict new %FC values for the same input set of core O/F, P_c, and T_{aw}. The improved coefficients are shown in Table 1, and the T_{aw} values for the initial and corrected coefficients are shown in Figure 3. From Figure 3 it was clear that these new values improved the accuracy of the equation; the maximum error on any measurement was reduced to 6%. It is notable that the values for the 30 kN engine had the same magnitude of error as those for the 3 kN engine, indicating that this equation could be valid for a range of engine sizes.

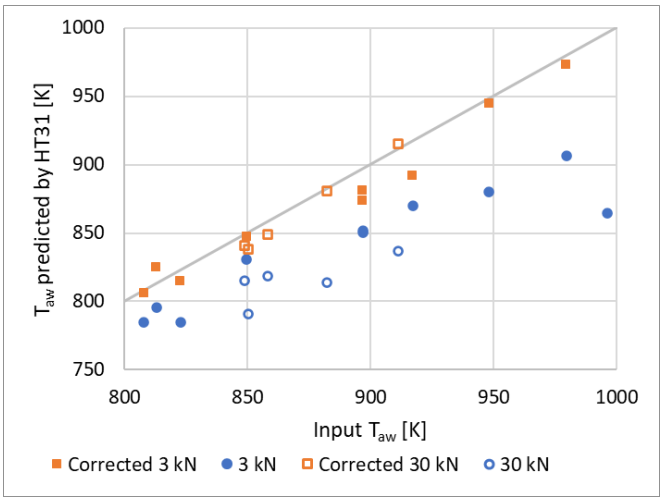

Figure 3: Plot of T_{aw} used to calculate the input %FC, against the T_{aw} returned by the HT31 program using the initial coefficients (blue) and corrected coefficients (orange)

Table 1: Updated coefficients for Equation 3

Coefficient	Value	Standard deviation
a	4.31×10^{-1}	2.1×10^{-2}
b	-3.69×10^{-2}	7.9×10^{-3}
c	7.16×10^{-3}	7.7×10^{-4}
d	-5.70×10^{-1}	2.3×10^{-2}

3.3. Performance trade-off

The specific impulse, I_{sp}, was calculated for a film-cooled engine via:

$$I_{sp} = C_f C^*_{total} = C_f\left(C^*_{core}(1 - \%FC) + C^*_{film}\%FC\right) \quad 4$$

Numerical evaluation was carried out via Matlab for target adiabatic wall temperatures of 700-1000K. Preliminary plots of I_{sp} as a function of core O/F and chamber pressure indicated that the range of O/F ratios and chamber pressures needed to be expanded to adequately display maxima in the data. Re-evaluation of the preliminary data collected for O/F 1.60 (at chamber pressures 3.8 MPa and 10.0 MPa, %FC 10, 20, and 30%) indicated that Equation 3 was still valid: the difference between calculated and simulated T_{aw} for a given %FC was within 10%, in line with the data from O/F 2.20-2.80. It was therefore considered reasonable to extend the calculation down to O/F 1.20 (the relationships found for C*, T_c and so on were invalid below this point). The chamber pressure range was also extended to 12 MPa to ensure that the surface maximum was found. Scenarios for which negative film cooling was calculated (i.e. for which the calculated core temperature was lower than the target T_{aw}) were removed and appear white on the graphs.

From the plots of different T_{aw} (Figure 4) it was seen that the peak region gradually shifted to a higher O/F value with decreasing temperature. The graphs showed very little variation in I_{sp} with core O/F, but a large change with chamber pressure; this was consistent with the trends seen in Figure 1 and Figure 2. The breadth of the peaks indicated low sensitivity to pressure and O/F changes within that range, enabling designers to choose core O/F and chamber pressure partially based on other factors (such as material availability or environmental factors) without an excessive reduction in performance. It was also evident that I_{sp} was roughly proportional to T_{aw}. Therefore, a higher wall temperature was desirable.

3.4. Engine condition determination

For a maximum wall temperature of 875 K, the I_{sp} was plotted (Figure 5) and showed a peak of I_{sp} 2576 m/s at core O/F 1.5 and P_c 10.35 MPa (although there was very little variation from P_c 9.5-11.5). However, there was a second peak of 2569 m/s at core O/F 2.48, P_c 8.75 MPa – again with a range of O/F 2.44-2.52, 8.55-8.95 MPa. The most significant difference between these two peaks was the %FC: the higher peak at lower core O/F had around 11.5% film cooling, whilst for the lower peak at core O/F 2.5 the amount of film cooling was around 27%. However, both had mass flow rates of 1.23 kg/s and so there was no change in the quantity of propellant required.

With an I_{sp} difference of less than 1%, and equal mass flow rates, it was decided to proceed with the higher core O/F: a greater quantity of oxidiser in the engine would lead to more complete combustion and reduce the quantity of pollutants such as particulate carbon and carbon monoxide (CO).

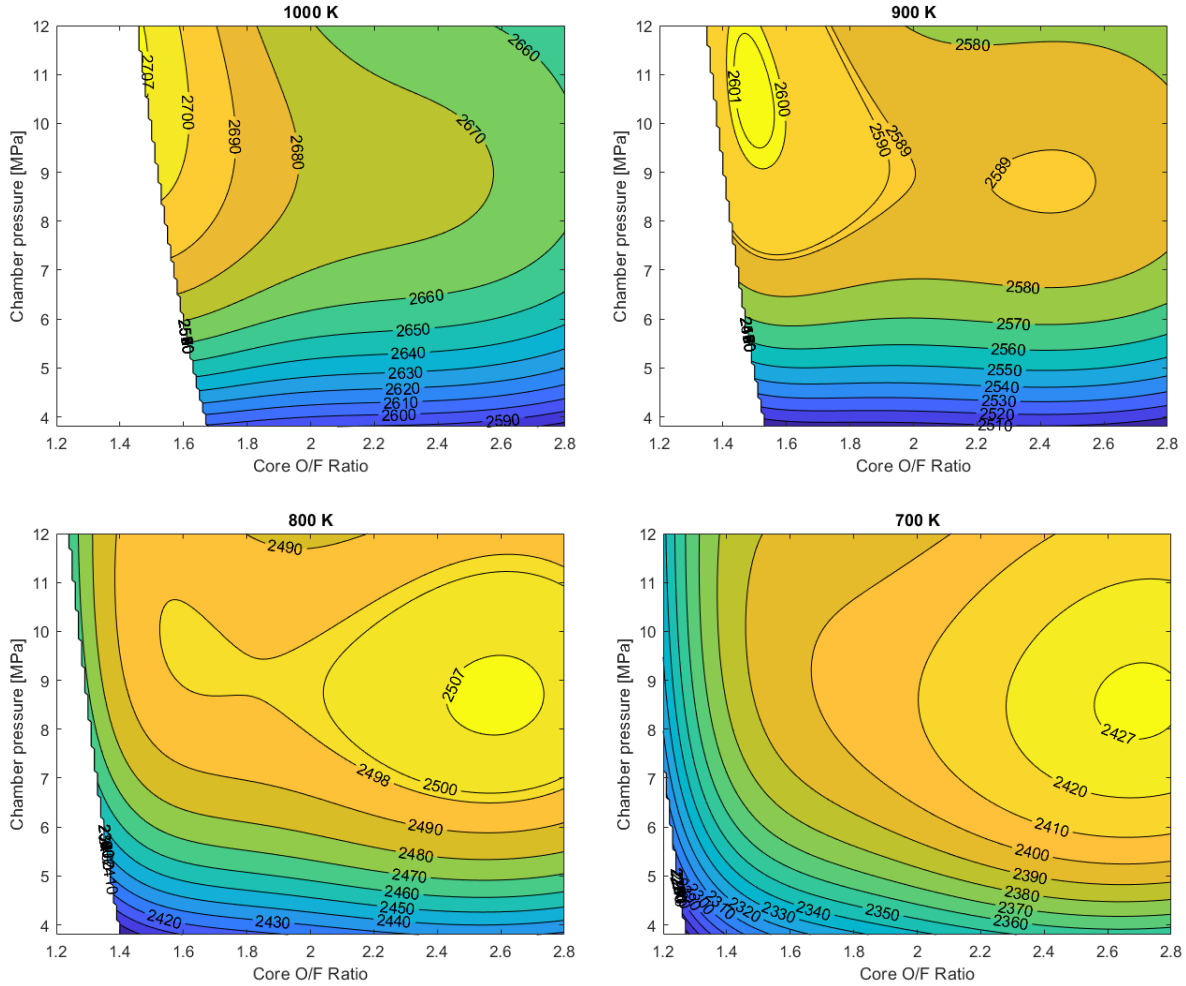

Figure 4: Plots of I_{sp} with extended O/F and P_c range, for target adiabatic wall temperatures of 1000 K, 900 K, 800 K, and 700 K (top left, top right, bottom left and bottom right, respectively)

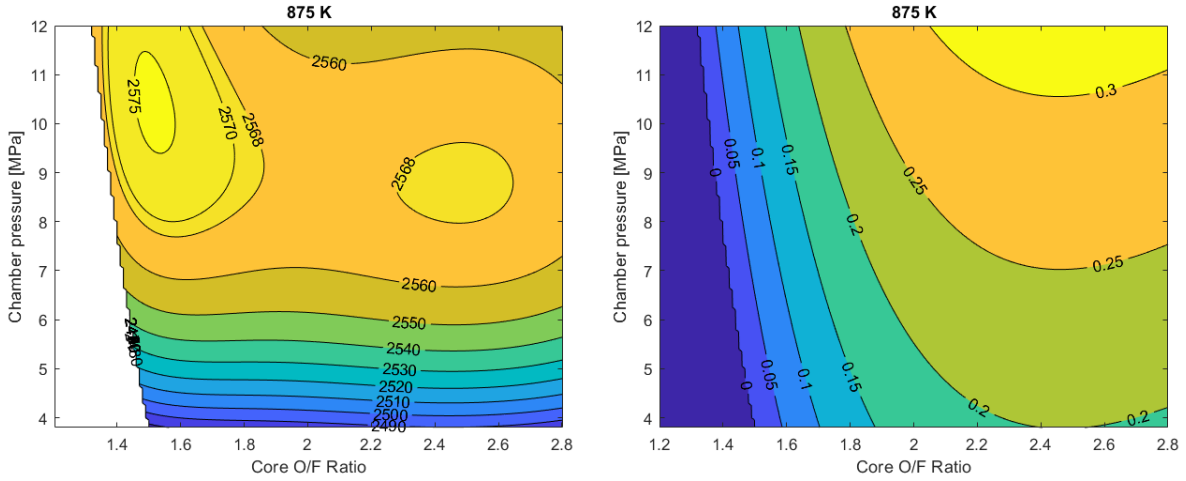

Figure 5: Plot of I_{sp} (left), and required film cooling (right), with O/F ratio and chamber pressure at the final design chamber wall temperature, 875 K

4. Conclusions

This project demonstrated a method to rapidly estimate the film cooling required for a LOX/butane engine. Numerical heat transfer modelling of several LOX/butane engines was used to determine an initial relationship between core O/F, chamber pressure, and target adiabatic chamber wall temperature. This heat transfer relationship was used to model engine I_{sp} for a range of O/F and P_c. For a maximum chamber wall temperature of 875 K, the optimal engine core O/F of 2.48 was found, corresponding to a chamber pressure of 8.75 MPa, 27% film cooling, and an I_{sp} of 2569 m/s. Simulations on random combinations of O/F, chamber pressure, and film cooling determined that the equation could predict the chamber wall temperature to within around 6%, equally well for a 3 kN or 30 kN engine.

This project was built entirely on simulated data, and while the modelling software used (RPA, HT31) have themselves been validated against real engines, practical data would be required to determine to what extent the film cooling equation could be used as a predictive tool for chamber temperature.

Acknowledgements

The author wishes to thank Professor Bob Parkinson for his guidance and mentorship, and for providing the HT31 programs; as well as the Cranfield Air and Space Propulsion Institute for supporting the author's attendance at EASN.

References

[1] J. Wink, R. Hermsen, R. Huijsman, C. Akkermans, L. Denies, F. Barreiro, A. Schutte, A. Cervone and B. Zandbergen, "Cryogenic rocket engine development at Delft aerospace rocket engineering," *Space Propulsion,* p. 3124644, 2016.

[2] Delft Aerospace Rocket Engineering (DARE), "Project Sparrow," June 2022. [Online]. Available: https://dare.tudelft.nl/project-sparrow/.

[3] B. Kanda, "Design, Build and Test-fire of a Nitrous Oxide-Isopropanol Liquid Sounding Rocket Engine," Cranfield University, 2022.

[4] J. G. Campbell, D. R. Batha, M. D. Carey, A. R. Nagy and R. C. Stechman, "Report 5981, Volume II: Thrust Chamber Cooling Techniques for Spacecraft Engines," The Marquardt Corporation, 1963.

[5] A. W. Miranda and M. H. Naraghi, "Analysis of Film Cooling and Heat Transfer in Rocket Thrust Chamber and Nozzle," in *49th AIAA Aerospace Sciences Meeting*, Orlando, Florida, 2011.

[6] B. A. Younglove and J. F. Ely, "Thermophysical Properties of Fluids. II. Methane, Ethane, Propane, Isobutane, and Normal Butane," *Journal of Physical Chemistry Reference Data,* vol. 16, no. 4, pp. 577-798, 1987.

[7] National Institute of Standards and Technology (NIST), "NIST Chemistry WebBook," April 2022. [Online]. Available: https://webbook.nist.gov/chemistry/.

[8] A. Herbertz, M. Ortelt, I. Muller and H. Hald, "Transpiration-Cooled Ceramic Thrust Chamber Applicability for High-Thrust Rocket Engines," in *48th AIAA/ASME/SAE/ASEE Joint Propulsion Conference & Exhibit*, Atlanta, Georgia, 2012.

[9] W. D. Jenkins, T. G. Digges and C. R. Johnson, "Tensile Properties of Copper, Nickel, and 70-Percent-Copper-30-Percent-Nickel and 30-Percent-Copper-70-Percent Nickel Alloys at High Temperatures," *Journal of Research of the National Bureau of Standards,* vol. 58, no. 4, pp. 201-211, 1957.

[10] High Temp Metals, “INCONEL 625 TECHNICAL DATA,” August 2022. [Online]. Available: https://www.hightempmetals.com/techdata/hitempInconel625data.php.

[11] Special Metals, “INCONEL alloy 625,” August 2022. [Online]. Available: https://www.specialmetals.com/documents/technical-bulletins/inconel/inconel-alloy-625.pdf .

[12] A. Ponomarenko, “RPA - Tool for Rocket Propulsion Analysis,” 2017. [Online]. Available: http://www.propulsion-analysis.com/.

[13] D. G. Hyams, “CurveExpert Professional,” April 2022. [Online]. Available: https://www.curveexpert.net/products/curveexpert-professional/.

[14] Z. A. R. Ashford, “Design of a 3 kN LOX/Hydrocarbon Film-Cooled Demonstration Engine,” Cranfield University, 2022.

[15] D. K. Huzel and D. H. Huang, Modern Engineering for Design of Liquid-Propellant Rocket Engines, A. R. Seebass, Ed., Progress in Astronautics and Aeronautics, 1992.

[16] R. W. Humble, G. N. Henry and W. J. Larson, Space Propulsion Analysis and Design, McGraw-Hill Companies, Inc., 1995.

[17] S. R. Shine and S. S. Nidhi, “Review on film cooling of liquid rocket engines,” *Propulsion and Power Research,* vol. 7, no. 1, pp. 1-18, 2018.

[18] J. M. Prakash, R. K. E. Roy, T. S. Krishnakumar, G. Remesh, J. C. Pisharady, P. Balachandran and R. P. Thomas, “Numerical Studies on Combustion in a Film Cooled Semi-Cryogenic Rocket Thrust Chamber,” in *48th AIAA/ASME/SAE/ASEE Joint Propulsion Conference & Exhibit*, Atlanta, Georgia, 2012.

[19] B. Parkinson, *The HT-31 Rocket Engine Heat Transfer Program(s), Version 4.0,* 2014.

[20] H. Ziebland and R. C. Parkinson, Heat Transfer in Rocket Engines, Aeronautical Research Council, 1972.

[21] W. Tabakoff and R. Ravuri, “Film Cooling Effectiveness for Combustion Chambers,” in *AIAA 13th Aerospace Sciences Meeting*, Pasadena, California, 1975.

[22] Y. C. Yu, R. Z. Schuff and W. E. Anderson, “Liquid Film Cooling Using Swirl in Rocket Combustors,” in *40th AIAA/ASME/SAE/ASEE Joint Propulsion Conference and Exhibit*, Fort Lauderdale, Florida, 2004.

[23] D. I. Suslov, R. Arnold and O. J. Haidn, “Investigation of Film Cooling Efficiency in a High Pressure Subscale LOX/H2 Combustion Chamber,” in *47th AIAA/ASME/SAE/ASEE Joint Propulsion Conference and Exhibit*, San Diego, California, 2011.

[24] High Temp Metals, “INCONEL 718 TECHNICAL DATA,” August 2022. [Online]. Available: https://www.hightempmetals.com/techdata/hitempInconel718data.php.

[25] Special Metals, “Inconel Alloy 718 SMC-045,” August 2022. [Online]. Available: https://www.specialmetals.com/documents/technical-bulletins/inconel/inconel-alloy-718.pdf.

2024-03-13

Analysis of film cooling for a 3kN LOX/butane demonstrator engine

Ashford, Zoe A. R.

IOP Publishing

Ashford ZAR. (2024) Analysis of film cooling for a 3kN LOX/butane demonstrator engine.
Journal of Physics: Conference Series Volume 2716, Issue 1, March 2024, Article Number 012088
https://doi.org/10.1088/1742-6596/2716/1/012088